Journal of The Electrochemical Society

Benefits of Fast Battery Formation in a Model System

Journal of The Electrochemical Society, 2021 **168** 050543

Benefits of Fast Battery Formation in a Model System

Peter M. Attia,[1,*,z] Stephen J. Harris,[1,2] and William C. Chueh[1,*,z]

[1]*Department of Materials Science and Engineering, Stanford University, Stanford, California 94305, United States of America*
[2]*Energy Storage Division, Lawrence Berkeley National Laboratory, Berkeley, California 94720, United States of America*

Lithium-ion battery formation affects battery cost, energy density, and lifetime. An improved understanding of the first cycle of solid-electrolyte interphase (SEI) growth on carbonaceous negative electrodes could aid in the design of optimized formation protocols. In this work, we systematically study SEI growth during the formation of carbon black negative electrodes in a standard carbonate electrolyte. We show that the initial ethylene carbonate (EC) reduction reaction occurs at ~0.5–1.2 V during the first lithiation, except under fast lithiation rates (⩾10C). The products of this EC reduction reaction do not passivate the electrode; only the SEI formed at lower potentials affects the second-cycle Coulombic efficiency. Thus, cycling quickly through the voltage regime of this reaction can decrease both formation time and first-cycle capacity loss, without an increase in subsequent-cycle capacity loss. We also show that the capacity consumed by this reaction is minimized at low temperatures and low salt concentrations. Finally, we discuss the mechanism behind our experimental results. This work reveals the fundamental processes underlying initial SEI growth on carbonaceous negative electrodes and provides insights for both optimizing the battery formation process and enabling novel electrolytes.

 [DOI: 10.1149/1945-7111/abff35]

Manuscript submitted March 21, 2021; revised manuscript received April 22, 2021. Published May 27, 2021.

Supplementary material for this article is available online

Improving the energy density, lifetime, and cost of lithium-ion batteries is critical to enable the electrification of transportation and grid storage.[1–3] In commercial batteries, all three of these factors are influenced by the formation and aging process, a key step in battery production.[4–7] One of the primary objectives of formation is to create a passivating, low-impedance solid-electrolyte interphase (SEI) layer on the graphitic negative electrode, which is ubiquitous in modern lithium-ion batteries. However, irreversible capacity loss during battery formation increases the positive electrode material required to compensate for the lost lithium inventory, which decreases the energy density and increases the cost (the positive electrode is among the most expensive battery components[5]). Additionally, the time required for formation increases the battery cost, as both the manufacturing time and formation cycling capital expense are substantial in cell manufacturing.[5] Finally, a poorly passivating SEI created during formation decreases the lifetime due to capacity consumption from further SEI growth.[6,8–11] As formation impacts these key battery metrics, designing rapid yet effective formation protocols is an important and active area of research.[12–20] A deeper understanding of formation cycle reactions will aid in these optimization efforts.

The first lithiation of graphite, and its accompanying side reactions, has been extensively studied. In fact, the challenges of lithium intercalation into graphite delayed the commercial introduction of lithium-ion batteries by around 20 years; Xu[10] and Winter et al.[21] provide in-depth reviews that discuss the centrality of this reaction to lithium-ion battery history. Electrolytes based on propylene carbonate (PC) were found to perpetually reduce during the first lithiation (typically[9] at around 0.8 V vs Li^+/Li^0), co-intercalating into and exfoliating the graphite particles indefinitely; if left unchecked, this reduction consumes all available lithium inventory while generating propylene gas.[8–10,21–27] In contrast, the use of ethylene carbonate (EC)-based electrolytes enabled reversible lithium intercalation into graphite and thus the commercialization of modern lithium-ion batteries.[10,21,28] However, EC electrolytes can also co-intercalate into, and exfoliate, graphite, and their concurrent reduction leads to major irreversible capacity loss.[8,10,11,21,29,30] The reported products of this reduction are ethylene gas[31–34] and a solid-phase carbonate, either lithium ethylene dicarbonate, LEDC ([35,36]), or lithium ethylene monocarbonate, LEMC ([37]). This coupled co-intercalation, reduction, and exfoliation occurs when solvated lithium ions (i.e., $Li^+(EC)_4$) co-intercalate at the "non-basal-plane" graphite surfaces, i.e., edge planes and defect sites.[38–40] Furthermore, the reduction of EC specifically (and not other electrolyte components) was linked to its presence in the lithium-ion solvation sheath[41–45] and supported by electrolyte composition[31,46] and gas generation[33,34,47,48] experiments. Additional studies have revealed that the irreversible capacity loss from this reaction increases with graphite heat treatment,[31–33,49] increases with applied pressure,[33] and decreases with the use of other cyclic carbonate electrolyte additives such as vinylene carbonate (VC) and fluoroethylene carbonate (FEC).[8,10,50–53] Finally, while the number of electrons transferred in the EC reduction reaction is somewhat controversial, most ab-initio studies[54–58] and our previous experimental work[48] have identified that two-electron pathways are most probable.

While the complex mechanistic details and the ordering of the co-intercalation, reduction, and exfoliation steps are still under investigation via both theoretical[56,59] and experimental[59,60] approaches, controlling this process is clearly important for optimizing lithium-ion battery formation. Throughout this paper, we refer to these combined steps occurring at high potentials of the carbon electrode (typically between 0.5 V–1.0 V) during the first lithiation as the "EC reduction" reaction, though we note that EC may also reduce at lower carbon potentials as well.

Despite this progress, however, translating these fundamental insights into design principles for optimized formation protocols is not straightforward. Märkle et al.[47] and Goers et al.[61] found that high currents (320 mA g^{-1}) during the first lithiation suppressed graphite exfoliation, but the use of moderate currents (40–160 mA g^{-1}) was found to deposit highly localized and nonuniform SEI. From a device perspective, previous studies on multistep formation protocols have indicated the importance of spending time at high cell potential (i.e., low graphite potentials) to form a well-passivating SEI and thus improve lifetime.[13,15] For instance, An et al.[13] achieved high capacity retention with formation protocols that performed shallow cycling at high cell potentials while minimizing the time spent at low cell potentials. Similarly, Antonopoulos et al.[17,18] suggested minimizing the time spent at high negative electrode potentials to decrease formation time. These results are consistent with the large body of work demonstrating the passivating ability of

*Electrochemical Society Member.
[z]E-mail: peter.m.attia@gmail.com; wchueh@stanford.edu

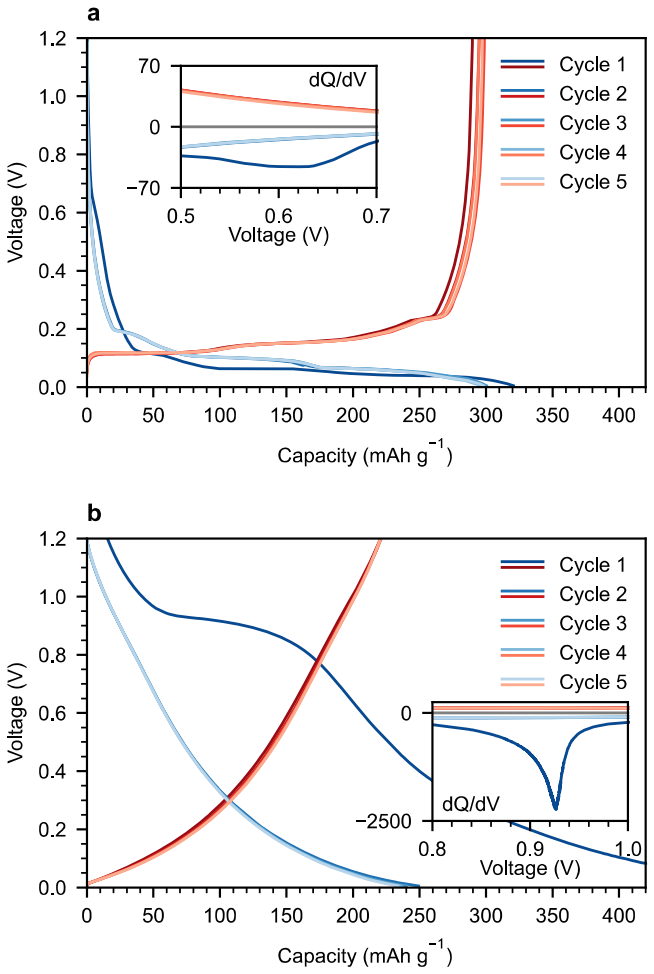

Figure 1. Comparison of the first five cycles for (a) graphite and (b) carbon black half cells cycling at C/10. Differential capacity (*dQ*/*dV*, units of mAh g^{-1} V^{-1}) vs voltage is displayed in the insets. The EC reduction peak is much larger on carbon black than graphite and occurs at a potential ~300 mV higher on carbon black than graphite. Additionally, this EC reduction reaction only occurs during the first lithiation.

SEI formed at low graphite potentials.[11,62–65] However, these applied results are somewhat difficult to generalize into more fundamental design principles for formation. Systematic studies of the dependence of the EC reduction reaction on process parameters like current and temperature could reveal both fundamental and applied insights into formation.

In this work, we perform systematic electrochemical characterization of the EC reduction reaction on carbon black, a high-surface-area model system for SEI growth.[48,66,67] We first compare the first lithiation (subsequently termed "formation") of carbon black to that of graphite. We then examine SEI growth as a function of formation current. When the current used in the EC reduction potential regime (~1.2 V–0.5 V) is large and the subsequent lithiation current (~0.5 V–0.01 V) is small (i.e., two-step formation), both the first-cycle irreversible capacity loss and the formation time are decreased, with no impact on lifetime (as quantified by the Coulombic efficiency of subsequent cycles). In fact, the amount of irreversible capacity loss within the EC reduction regime has no effect on the Coulombic efficiency of subsequent cycles. This result indicates that the products of EC reduction do not passivate the electrode. We then characterize the behavior of EC reduction as a function of temperature and electrolyte salt concentration, finding that low temperatures and low salt concentrations decrease the irreversible capacity loss of the EC reduction reaction. Finally, based on linear sweep voltammetry results, we propose that high rates and low temperatures suppress the detrimental effects of EC reduction because EC reduction becomes diffusion limited before carbon lithiation. This work reveals fundamental insights underlying the initial formation of SEI and illustrates pathways for improving formation cycling and electrolyte design in lithium-ion batteries with carbonaceous negative electrodes.

Experimental

Cell fabrication.—Carbon black slurries were prepared using TIMCAL Super P and polyvinylidene difluoride (PVDF) binder (Alfa Aesar) in a 90:10 wt.% ratio with NMP solvent (Sigma-Aldrich). Slurries were mixed with a planetary mixer (THINKY AR-100), cast at a nominal thickness of 100 μm on 18 μm thick electrodeposited copper foil (Hohsen), and dried overnight (~12 h) in a vacuum oven at 55 °C. The final stack thickness (electrode + copper foil) was 45–55 μm, as measured with a micrometer.

Electrode disks (13 mm diameter, 1.33 cm^2 geometric area) were then punched for coin cell assembly and weighed on an analytical microbalance (Mettler-Toledo XPR2). The active carbon black mass loading is approximately 0.6 mg cm^{-2} (0.8 mg per disk). The cells were assembled in an argon glove box (VAC, <1 ppm O_2 and <0.5 ppm H_2O) using stainless steel 2032 coin cell cases (Hoshen) with 50 μl of 1.0 M $LiPF_6$ in EC:DEC (1:1) by weight (BASF/Gotion Selectilyte LP40), one 25 μm separator (Celgard) and a lithium foil (Alfa Aesar) counter electrode. The geometric volume of the carbon black electrodes is ~4 μl (1.33 cm^2 × 32 μm. We note that these values yield a theoretical electrode porosity of 88%; see our previous work[66] for electron micrographs of the highly porous structure of this electrode. The electrolyte volume is ~4 ml g^{-1}, well in excess of the electrode volume (~12.5×). We selected a large electrolyte-to-electrode ratio because the concentrations of SEI intermediates and products scale with surface area, and our carbon black electrodes have a high surface area.

The graphite electrode presented in Fig. 1 was extracted from a dry, unformed A123 20 Ah lithium iron phosphate (LFP)/graphite pouch cell (AMP20M1HD-A); the particles from one side of the double-sided electrode were removed using a cotton swab soaked in isopropyl alcohol, and then the coin cell was constructed as described in the preceding paragraph. In experiments where we vary the salt concentration, solutions of varying molality were created using $LiPF_6$ (≥99.99%, Sigma Aldrich), ethylene carbonate, EC (99%, anhydrous, Sigma Aldrich), and diethyl carbonate, DEC (≥99%, Sigma Aldrich). The chemicals were used as-received.

Electrochemical characterization.—Cells were generally cycled inside a temperature chamber (AMEREX IC-150R) at a constant nominal temperature of 30.0 °C (±0.5 °C) with a Bio-logic BCS-805. In experiments where we increase the temperature beyond 30 °C, the cells were cycled in silicone oil baths heated by hot plates, and the temperature was monitored via thermocouples. Unless otherwise specified, all cells were charged and discharged at a constant current between 1.2 and 0.01 V, with no potentiostatic hold at either cutoff potential. All C rates for carbon black electrodes were calculated using a specific capacity of 200 mAh g^{-1} (1C = 200 mA g^{-1}_{CB}),[66] which corresponds to a current density of ~3.2 mA m^{-2}_{CB} (geometric area) given a specific surface area of 62 m^{-2} g^{-1}.[48] All C rates for graphite electrodes were calculated with a specific (theoretical) capacity of 372 mAh g^{-1} (1C = 372 mA g^{-1}_{CB}),[68] which corresponds to a current density of ~372 mA $m^{-2}_{graphite}$ (geometric area) given a specific surface area of 1.0 m^{-2} g^{-1} (measured). All cells rest for 24 h before cycling to ensure complete electrolyte wetting.

Results

Comparison of first-cycle reactions of carbon black and graphite.—Graphite is the most commonly used negative electrode material in commercial lithium-ion batteries. Other carbon materials

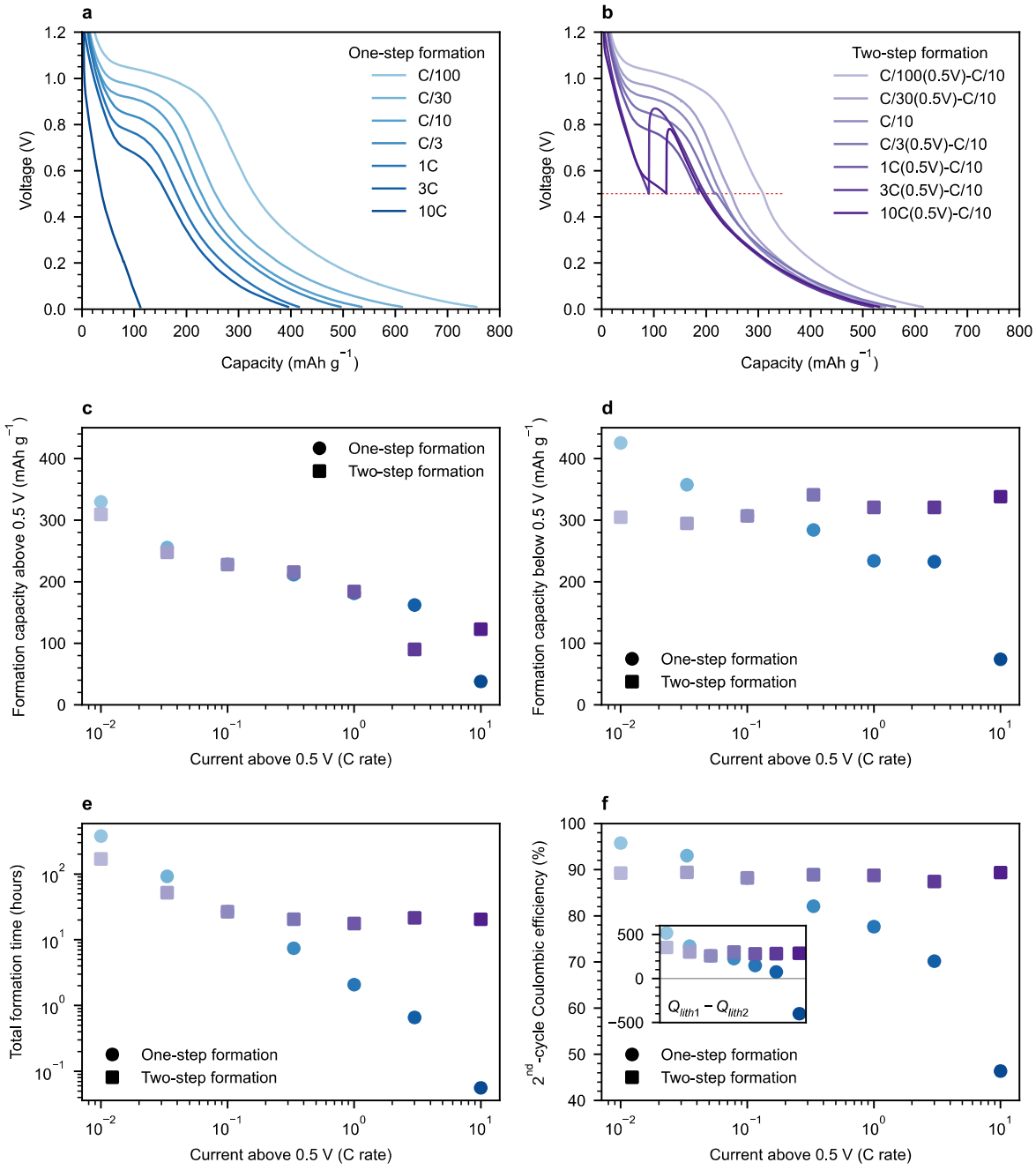

Figure 2. Two experiments to probe first-cycle SEI growth (formation) on carbon black. (a) Voltage vs capacity for the one-step formation experiment. For these cells, a single current ranging from C/100 to 10C is applied throughout the first lithiation. (b) Voltage vs capacity for the two-step formation experiment. For these cells, a current also ranging from C/100 to 10C is applied until 0.5 V, after which all cells complete lithiation at C/10. (c), (d) The formation capacity (i.e., first lithiation) (c) above and (d) below 0.5 V for both experiments as a function of the current above 0.5 V (i.e., the current for one-step formation and the first current for two-step formation). The above-0.5 V formation capacities closely match each other, while the below-0.5 V formation capacities are clearly a function of C rate. Note that in the two-step formation experiment, the formation capacity above 0.5 V during the second step (i.e., due to overpotential relaxation) is excluded from both quantities. (e) Total formation time (i.e., first lithiation time) for both experiments as a function of the current above 0.5 V (i.e., the current for one-step formation and the first current for two-step formation). (f) Second-cycle Coulombic efficiency (CE) for both experiments as a function of the current above 0.5 V (i.e., the current for one-step formation and the first current for two-step formation). The inset displays the difference between the lithiation capacities of the first and second cycles (units of mAh g^{-1}). All cycling after the first lithiation occurred at a rate of C/10. The second-cycle CE for the one-step current experiment decreases with increasing C rate, while the second-cycle CE is independent of the rate of the first step in the two-step formation experiment.

such as carbon black grow significantly more SEI per cycle. Here, we take advantage of this property, which enables more quantitative measurements of SEI growth. Other authors have studied SEI growth on carbon black, often in the context of its widespread use as a conductive electrode additive;[46,66,69–74,67] our previous work on "post-first-cycle" SEI growth[66] details relevant differences between graphite and carbon black. Importantly, carbon blacks "differ only in the magnitude of their variation from graphite rather than representing different crystallographic structures" (Donnet et al.[75]), and our previous characterization work[66] reveals similar surface chemistry between carbon black and graphite. Furthermore, Smith et al.[73] reported similar rates of post-first-cycle areal capacity loss between graphite and carbon black, even though the basal plane:edge plane ratio was not controlled between the two materials. Finally, we note

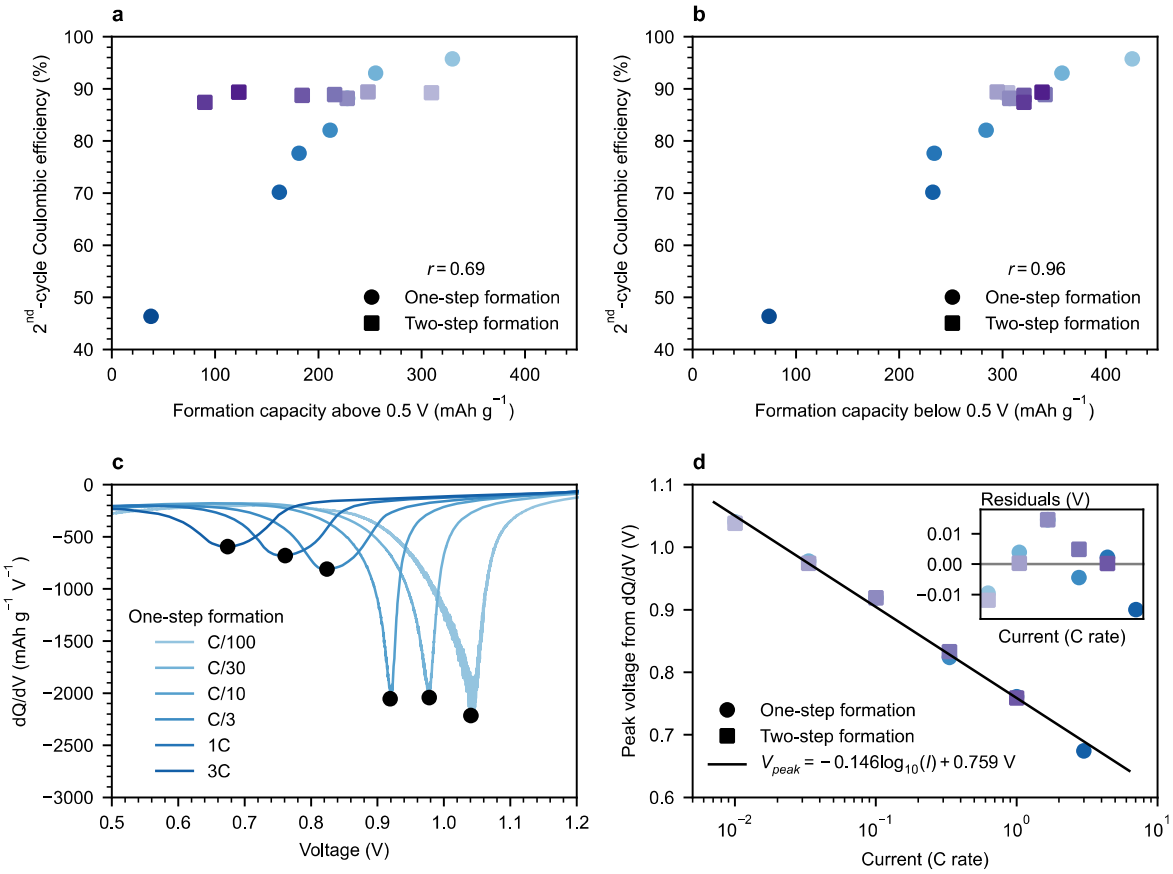

Figure 3. Additional analysis of the one-step and two-step formation experiments. (a), (b) Correlation between 2nd-cycle Coulombic efficiency (CE) and the (a) above-0.5 V formation capacities and (b) below−0.5 V formation capacities. The correlation coefficient, *r*, is displayed above the legends. Note that in the two-step formation experiment, the formation capacity above 0.5 V during the second step (i.e., due to overpotential relaxation) is excluded from both quantities. (c) *dQ/dV* vs voltage for the one-step formation experiment. The peak voltage decreases from 1.04 V at C/100 to 0.67 V at 3C. The decreasing size of the EC reduction peak with increasing C rate is clearly visible. (d) Peak voltage from *dQ/dV* vs voltage from both the one-step and two-step formation experiments. The peak potential and the log of current have a linear relationship, indicating that the reaction is electrochemically irreversible; the residuals of the fit are displayed in the inset.

that the gaseous products of the EC reduction reaction (namely, ethylene) are identical for these materials.[33,47,48] Overall, carbon black serves as a good, albeit imperfect, model system for fundamental investigations of SEI growth; however, we acknowledge that other differences may limit the applicability of our carbon black results to graphite systems. We discuss the impact of some of these differences throughout the manuscript.

Figure 1 presents voltage vs capacity and for graphite and carbon black half-cells cycling at C/10. Differential capacity (*dQ/dV*) vs voltage is presented in the insets. The most immediate observation is the difference in magnitude of the first-cycle EC reduction peaks; the peak differential capacity is 49× larger in carbon black than in graphite (neglecting differences in differential capacity from the "background" signal of lithiation). We attribute this difference primarily to the much larger specific surface area of carbon black relative to graphite (62 $m^2\ g^{-1}$ vs ∼1.0 $m^2\ g^{-1}$).[48,66] The large size of this peak in carbon black motivates our use of this material in this work; the exaggerated capacity loss of EC reduction enables easier visualization of the dependences of this reaction. However, given the small size of this peak in graphite, we emphasize that controlling the EC reduction reaction is only one lever for optimizing formation of graphitic negative electrodes.

Additionally, the peak voltage at C/10 increases from ∼0.6 V in graphite to ∼0.9 V in carbon black. We attribute this 300 mV difference in peak position to the additional overpotential from the higher current density of graphite relative to carbon black. The current density of graphite at C/10 is ∼37 mA m^{-2} (37.2 mA g^{-1}/1 $m^2\ g^{-1}$), while the current density of carbon black at C/10 is ∼0.32 mA m^{-2} (20.0 mA g^{-1}/62 $m^2\ g^{-1}$). In fact, from our eventual quantification of the relationship between peak potential and current in carbon black (Fig. 3d), the peak potential scales with −0.146 V x $\log_{10}(I)$; thus, a ∼115× increase in current density (∼37.2 mA m^{-2}/∼0.322 mA m^{-2}) precisely explains a 300 mV decrease in peak potential (∼0.146 V × $\log_{10}(115)$ = 301 mV). The ∼5% larger interplanar spacing of carbon black relative to graphite[66,75,76] does not appear to contribute to the decreased overpotential in carbon black, even though larger interplanar spacing may enable more facile solvent cointercalation. This result gives us further confidence in the similarities of the EC reduction reaction between graphite and carbon black.

Importantly, in both graphite and carbon black, the EC reduction reaction appears to be confined to the first lithiation. We do not observe peaks in this potential regime during all subsequent (de) lithiations, except for subsequent cycles with exceptionally high first-lithiation currents (i.e., 10C; see Fig. S1 available online at stacks.iop.org/JES/168/050543/mmedia). This result is consistent with measurements showing gas generation only during the first lithiation of carbon negative electrodes.[34,48] Thus, the EC reduction reaction is distinct from subsequent-cycle SEI growth, and even from SEI growth at low potentials during the first lithiation. We note that both types of growth are examples of electrochemical SEI growth.[77] Chemical SEI growth may also play a role in this system, but its growth is much slower (∼0.2 mA g^{-1} capacity loss rate from chemical SEI growth during the second cycle)[77] than subsequent-cycle electrochemical SEI growth (∼3 mA g^{-1} capacity loss rate from electrochemical SEI growth during the second cycle at C/10).[66]

Furthermore, chemical SEI growth slows with increasing potential, i.e., decreasing lithium concentration (~0.05 mA g^{-1} capacity loss rate from chemical SEI growth during the second cycle from ~0.3 V to ~0.4 V)[77] and is thus expected to be much slower at the potentials of the EC reduction reaction.

A final aspect to note is that carbon black has more reversible charge storage than graphite in the potential regime of EC reduction, i.e. from 0.5 V–1.0 V. In fact, the C/10 capacity of carbon black between 0.5 V and 1.0 V is 13× larger than that of graphite for the second lithiation (here we use the second lithiation to isolate the reversible charge storage capacity from that of irreversible EC reduction; the capacity in this voltage regime does not change appreciably with cycle number,[66] implying that the second-cycle capacity within this window can be used as a reliable measure of the reversible charge storage capacity). This difference will become relevant in our later discussions.

With these differences in mind, the remainder of our experiments are performed exclusively on carbon black. Note that the high electrode porosities and electrolyte volumes of our cells enable us to isolate the reaction kinetics of EC reduction and minimize other contributions to overpotential like mass transport, as confirmed by the excellent rate capability of the electrodes.[66]

Dependence on formation current.—We begin by systematically investigating the sensitivity of formation metrics (i.e., formation time, formation capacity loss, and subsequent-cycle capacity loss) to formation current. Figure 2 displays the results of two experiments with variable formation currents, termed the "one-step " and "two-step" formation experiments. In Fig. 2a, carbon black electrodes were lithiated at currents ranging from C/100 to 10C ("one-step" formation); these currents span three orders of magnitude. In contrast, the carbon black electrodes in Fig. 2b were lithiated at currents ranging from C/100 to 10C, but only until 0.5 V; below 0.5 V, the carbon black electrodes lithiated at C/10 down to the lower cutoff voltage ("two-step" formation). We use the nomenclature *X*(0.5 V)-C/10 to describe the two-step formation protocols: *X* represents the lithiation current until 0.5 V, which is followed by lithiation at C/10 to 0.01 V. For the two-step formation experiment, the cells with $X > C/10$ naturally exhibit a voltage step at the transition point. For both experiments, the size and location of the EC reduction plateau clearly depend on the magnitude of the current.

Figures 2c and 2d display the formation capacities (i.e., capacities measured during the first lithiation) above and below 0.5 V, respectively. Here we exclude the capacity above 0.5 V during the second step of two-step formation (i.e., due to overpotential relaxation after switching to a slower current) from both quantities. We find that the above-0.5 V formation capacities of the two experiments (Fig. 2c) are similar, with the exception of the values at high currents (3C and 10C). We attribute these capacity differences to variation in cell fabrication that become amplified at high rates. In contrast, the below-0.5 V formation capacities of the two experiments (Fig. 2d) diverge, as these capacities decrease with current for one-step formation but are relatively level for two-step formation.

For both experiments, the above-0.5 V formation capacities decrease with current. Of course, both the above- and below-0.5 V formation capacities have contributions from both lithiation and SEI growth. Excluding the 10C experiment, which does not exhibit an EC reduction peak, the formation capacities in the above-0.5 V potential regime for one-step formation range from 162 mAh g^{-1} at 3C to 330 mAh g^{-1} at C/100. Since the second-cycle lithiation capacity of carbon black between 0.5 V and 1.0 V is 58 mAh g^{-1} at C/10, we attribute most (64%–82%) of the above-0.5 V formation capacity to irreversible capacity loss from the EC reduction reaction. In fact, since the lithiation capacity at C/10 is much higher than that at 3C ([66]), even our lower bound of the fraction of irreversible capacity loss between 0.5 V and 1.0 V (64%) is certainly underestimated (i.e., 58 mAh g^{-1} is an overestimate of the lithiation capacity in this voltage range at 3C).

Figure 2e displays the total formation time (i.e., during the first lithiation) for both experiments. For one-step formation, the formation time naturally decreases with C rate. The measured time does not correspond to the expected time given the C rate (e.g., 10 h for C/10) due to the large capacity of the EC reduction reaction. In contrast, the lithiation time levels off at ~20 h for two-step formation, since the formation time below 0.5 V is fixed at C/10.

Figure 2f presents a key result of this paper: the second-cycle Coulombic efficiency for both experiments. We use this metric as a proxy for capacity retention over life. Initial Coulombic efficiency is generally predictive of capacity loss due to SEI growth,[73,78] the most common degradation mode in lithium-ion batteries, but of course other degradation modes that decrease lifetime may not be captured by Coulombic efficiency. The second cycle was selected due to its high sensitivity, although the trends in Coulombic efficiency persist until the fifth cycle (though somewhat convoluted by cell-to-cell variation; see Fig. S2). All cycling after formation occurred at a rate of C/10 to ensure a fair comparison between cells, since SEI growth rates in carbon black depend on the magnitude of the lithiation current.[66,67]

For one-step formation, the second-cycle Coulombic efficiency decreases with formation rate: decreasing the initial formation time clearly compromises the passivation ability of the first-cycle SEI (by passivation, we mean suppressing further SEI growth). In contrast, the second-cycle Coulombic efficiency for the two-step formation is essentially independent of the first formation step (that is, the current during the potential regime of EC reduction). Second-cycle voltage vs capacity for lithiation and delithiation are displayed for both experiments in Fig. S1. Since the curves are mostly overlapping except for some cell-to-cell variation (i.e., variation unordered by formation protocol), the irreversible capacity loss does not appear to measurably increase the impedance, at least at C/10.

Overall, the general trends in Fig. 2d closely match those of Fig. 2f. The implication of these results is that the EC reduction products at high potential provide *no* electrode passivation. While "porous SEI" formed at high potentials has been reported to be less passivating than "compact SEI" formed at low potentials,[11,62–65] the prevailing assumption in the field is that the passivation from the EC reduction products is needed to prevent further reduction.[8–11,21,30,79,80] However, we achieve appreciable lithiation capacity even with the 10C-C/10 two-step formation experiment, for which the EC reduction peak is not observed. Thus, the extent of the EC reduction reaction does not appear to influence subsequent-cycle Coulombic efficiency. In contrast, the benefits of formation capacity below 0.5 V are clear from Figs. 2d and 2f; the one-step cells with high formation capacity below 0.5 V (e.g., C/100 and C/30) also have high second-cycle Coulombic efficiency.

A possibility is that non-passivating EC reduction products formed at high potentials transform at low potentials and become passivating SEI. However, our results indicate that the extent of EC reduction at high potentials has little impact on the subsequent-cycle Coulombic efficiency. For instance, the C/100(0.5 V)-C/10 experiment and the 10C(0.5 V)-C/10 experiment have above-0.5 V formation capacities of 309 mAh g^{-1} and 123 mAh g^{-1}, respectively, but both experiments have nearly identical second-cycle Coulombic efficiencies (89.3% for C/100(0.5 V)-C/10 and 89.4% for 10C (0.5 V)-C/10). Thus, our results suggest that while the high-potential EC reduction products may reduce at low potentials, these transformed products also do not passivate the carbonaceous electrode.

The lack of passivation of the EC reduction products could be attributed to high porosity and/or high intrinsic material conductivity. Many previous reports[11,62,63] classify the high-potential SEI as porous; similarly, we observed large, amorphous deposits of "extended SEI" on carbon black in our previous work.[48] Additionally, Wang et al.[37] found that LEMC, a possible EC reduction product, has a moderate ionic conductivity ($>10^{-6}$ S cm^{-1}). Poor passivation ability may also help explain recent electrolyte exchange experiments indicating that the lithium-ion coordination structure of the new electrolyte is more important for minimizing capacity loss than the

SEI created by the original electrolyte.[81] Further chemical and morphological characterization of the SEI formed in formation may elucidate why these EC reduction products do not passivate the carbonaceous electrode.

While we do not characterize the rate capability as a function of formation protocol, the transport properties of the SEI may be influenced by the formation rate(s). A better understanding of the relationship between rate capability and formation protocol is the subject of future work. However, large volumes of SEI may decrease the electrode porosity and thus decrease the kinetics of bulk electrolyte transport, suggesting yet another advantage of using high currents in the EC reduction regime.

Overall, the results of the one-step and two-step formation experiments have clear implications for battery formation. Despite causing large amounts of irreversible capacity loss, the SEI from the EC reduction reaction provides no passivation ability; only the SEI products formed at low potential passivate the electrode. Thus, the use of high currents in the high-potential regime decreases the total time and irreversible capacity loss of the first cycle, which directly lowers cost and improves energy density with no discernible impact on lifetime.

Additional analysis of C rate dependence.—Figure 3 presents additional analyses of the one-step and two-step formation experiments. We quantified the strength of the linear correlation between the formation capacities above and below 0.5 V and the second-cycle Coulombic efficiency in Figs. 3a and 3b, respectively. We find that the correlation between the formation capacity at voltages >0.5 V and the second-cycle Coulombic efficiency is weak (r = 0.69, Fig. 3a). For two-step formation, the formation capacity at voltages >0.5 V is clearly uncorrelated with the second-cycle Coulombic efficiency. However, the correlation between the formation capacity at voltages <0.5 V and the second-cycle Coulombic efficiency is much stronger (r = 0.96, Fig. 3b). This result is consistent with the large body of work demonstrating the beneficial passivation ability of SEI products formed at low potential[11,62–65] and with previous work on two-step formation protocols.[13,15]

Figure 3c displays dQ/dV curves for one-step formation, with the exception of the 10C experiment (for which an EC reduction peak was not observed). The decrease in both peak potential and peak capacity at higher rates is evident. The peak potential from dQ/dV ranges from ∼0.65 V at 3C to ∼1.05 V at C/100. The sudden drop in peak dQ/dV from C/3 to C/10 likely reflects cell-to-cell variation and error introduced by numerical differentiation.

Figure 3d presents the peak potential from dQ/dV vs the nominal C rate above 0.5 V for both one-step and two-step formation. We find that the peak potential from dQ/dV has a linear relationship with the log of current; although dQ/dV is influenced by both carbon black lithiation and EC reduction, the peak potential is primarily influenced by EC reduction since carbon black lithiation is featureless in this voltage regime (Fig. 1b). Goers et al.[61] found that a similar relationship held for the onset potential of the EC reduction reaction in graphite. This behavior indicates that a reaction is electrochemically irreversible, that is, electron transfer from the reduced product back to the electrode is negligible (in contrast, the peak potential is invariant with current for an electrochemically reversible reaction).[82] In other words, charge transfer (i.e., EC reduction) is much slower than mass transport (i.e., transport of $Li^+(EC)_4$ to the surface of the carbon particles), and the reaction is exhibiting Tafel kinetics. Note that our cell design (i.e., thin electrodes, high electrode porosity, and high electrolyte volume) is designed to minimize mass transport overpotential within the electrolyte, so more realistic cell designs may have larger contributions from these sources of overpotential. We further consider the transport kinetics of EC reduction in the Discussion.

While quantification of electrochemical reaction parameters like exchange current density and equilibrium potential is not straightforward for galvanostatic experiments,[82] our results demonstrate that the reaction kinetics of EC reduction are slow. Because the overpotential appears to scale with the log of current even at the low rate of C/100, we conclude that the range of currents and peak potentials considered here are well above equilibrium values. For instance, the equilibrium potential in carbon black is likely well above 1.04 V (the peak potential at C/100); note that the literature often cites 0.8 V as a canonical equilibrium potential for this reaction on graphite,[9] which has higher overpotentials than carbon black due to its lower specific surface area (i.e., higher local current density for an equivalent C rate). Additionally, the exchange current density is likely much lower than C/100; for reference, rate testing of carbon black shows that the lithiation capacity drops noticeably only at currents above C/5 ([66]), so the kinetics of lithiation appear to be much faster than those of EC reduction. While we do not know the exact rate-limiting step in the EC reduction sequence, we expect this reaction to be slow due to its complexity (bulky cointercalation, bond-breaking reaction, two-electron reduction, etc.). Collecting data at even lower currents would enable a better understanding of these parameter values.

Because gas generation is highly favorable from a thermodynamic (entropic) perspective, we suspect that nearly all of the reduced Li^+-$(EC)_4$ intermediate participates in the subsequent chemical decomposition reaction to form ethylene gas and LEMC/LEDC.[56,57] Using the nomenclature of classical electrochemistry, we propose that EC reduction is an E_iC_i reaction, meaning an electrochemically irreversible reaction with a subsequent chemically irreversible reaction.

The robustness of the linear relationship in Fig. 3d (even at very slow currents) provides further evidence that the SEI formed by the EC reduction reaction is not passivating. If it were, we would expect increased error of the fit at low currents (i.e., when significant amounts of EC reduction products are formed) due to increased transport overpotential from self-passivation.

Optimization of both first-cycle and second-cycle capacity loss.—Thus far, we have largely focused on the role of the EC reduction reaction in formation optimization, demonstrating that the SEI formed at low potential ($V < 0.5$ V) entirely controls the second-cycle Coulombic efficiency. In formation, we want to minimize both the irreversible capacity loss from formation (minimized at high rates, Figs. 2c and 2d) and the irreversible capacity loss from cycling (minimized at low rates, Fig. 2f); we also want to minimize the formation time (Fig. 2e). These competing objectives can be optimized simultaneously. In Fig. 4, the combined irreversible capacity loss ($Q_{lith} - Q_{delith}$) of the first and second cycles is presented for (a) one-step formation and (b) two-step formation. For the first cycle, only the capacity below 0.5 V is used to exclude contributions from the EC reduction reaction, while the second cycle irreversible capacity loss includes the total capacity from lithiation and delithiation. Note that this objective only uses the second cycle irreversible capacity loss to represent capacity loss over life, but the capacity loss beyond the second cycle diminishes rapidly with cycle number (the average Coulombic efficiency rises from ∼89% at cycle 2 to ∼96% at cycle 5, Fig. S2).

In Fig. 4a, the irreversible capacity loss of the first cycle decreases with formation current; as the C rate increases, less time is spent at the potentials of appreciable SEI growth. Conversely, the irreversible capacity loss of the second cycle increases with formation current (the 10C value is anomalously high because EC reduction above 0.5 V occurs in the second cycle). The combined irreversible capacity loss is minimized for a C rate range between C/10 and 1C. On average, the first-cycle capacity loss is 7.6× larger than the second-cycle capacity loss, highlighting the sensitivity of battery lifetime to formation. Thus, the costs of very slow formation (C/100)—namely, high first-cycle irreversible capacity loss and long formation time—do not outweigh the benefits (low second-cycle capacity loss) compared to faster rates. Cycling too quickly (>1C), however, leads to large second-cycle irreversible capacity loss (and, of course, could lead to lithium plating). At these rates, lithiation is transport limited and thus little passivation occurs during the first

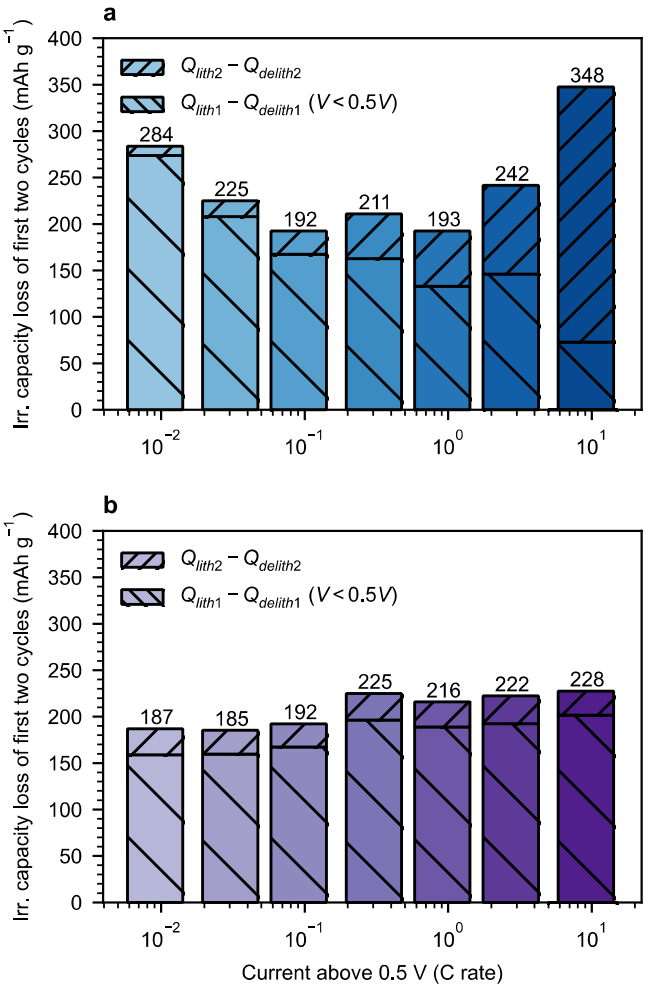

Figure 4. Irreversible capacity loss (lithiation capacity—delithiation capacity) of both the first and second cycle for (a) one-step formation and (b) two-step formation. For the first cycle, only the capacity below 0.5 V is used to exclude contributions from the EC reduction reaction, while the second-cycle irreversible capacity loss is the difference between the lithiation and delithiation capacities. The irreversible capacity loss of the first two cycles is minimized between C/10 and 1C for one-step formation and largely independent of formation current for two-step formation.

cycle. Overall, a formation current of ∼1C—that is, the highest rate achievable before lithiation becomes transport limited—appears to best minimize both irreversible capacity loss and formation time.

Figure 4b presents the combined irreversible capacity loss for two-step formation. As expected, both the first-cycle and second-cycle capacities are roughly constant, suggesting that the current above 0.5 V can be maximized without affecting lifetime. Note that the irreversible capacity loss of the first cycle is slightly higher (∼30 mAh g^{-1}) for cells with formation currents >C/10; we attribute this result to cell-to-cell variation. In summary, 10C(0.5 V)−1C appears to be the optimal formation protocol for this system.

Dependence on formation temperature and electrolyte salt concentration.—We also investigate the dependence of the EC reduction reaction on temperature and salt concentration (Fig. 5). Both of these dependences are fundamentally and technologically interesting. Unlike changing the applied current, temperature and salt concentration affect both the thermodynamics and kinetics of the reaction. Furthermore, temperature is a common parameter with which formation is controlled,[7,13,16] and electrolytes with high salt concentrations (typically >∼3–5 M)[83] are gaining interest due to their improved charge transfer kinetics and safety advantages.[83–85] Of course, the effect of salt concentration is not exclusive to formation (i.e., electrolyte design affects the rate capability, lifetime, etc., independent of its first-cycle effects).

Figure 5a displays voltage vs capacity for the formation of carbon black at temperatures ranging from 30 °C to 80 °C, with *dQ/dV* vs voltage displayed in the inset. The position and magnitude of the EC reduction reaction is sensitive to temperature. The peak potentials range from 0.90 V to 1.20 V, and the above-0.5 V formation capacities range from 217 mAh g^{-1} (30 °C) to 612 mAh g^{-1} (80 °C). These results indicate that using low temperatures when performing the EC reduction reaction during formation is optimal, although high temperatures may be optimal for the SEI reactions occurring below 0.5 V. However, other objectives of the formation process, like electrode wetting, may be best performed at high temperature, so these steps should be separated if possible.

We find that the peak potential from *dQ/dV* scales linearly with temperature (Fig. 5b), although the 80 °C peak potential appears to deviate slightly from the linear trend (see residuals plot in inset). Scaling relationships can typically be used to identify the dominant thermodynamic and kinetic factors in an electrochemical process. However, in this case, both the equilibrium potential and the reaction overpotential linearly scale with temperature (via the Nernst and Butler-Volmer/Tafel equations, respectively). Thus, in the absence of additional measurements, we cannot distinguish the contributions from these two mechanisms. However, given our previous conclusion that this reaction is electrochemically irreversible, we expect that the reaction kinetics are improved dramatically by high temperature and are a stronger determinant of the peak potential than the thermodynamic contribution. Another implication of this finding is that the transport kinetics of this process are less strongly influenced by temperature than the reaction kinetics, as transport processes typically have an Arrhenius scaling with temperature yet we observe a linear dependence on temperature. Additionally, we can assume the electrolyte transport overpotential is negligible (∼3 μV at 20 °C) from the applied current (C/10 ≈ 16 μA), cell geometry (cross-sectional area = 1.33 cm^2, separator thickness = 25 μm), and previously measured electrolyte transport properties (σ_{ionic} ≈ 10 mS cm^{-1} at 20 °C).[86]

We also explore the dependence of the EC reduction reaction on $LiPF_6$ salt concentration (Fig. 5c). Here, we use electrolytes with constant cosolvent ratios (1:1 EC:DEC by weight) but different concentrations of $LiPF_6$ (ranging from 0.5 m to 4.0 m). The location and magnitude of the EC reduction reaction is sensitive to salt concentration; the peak potentials range from 0.96 V (0.5 m) to 0.85 V (4.0 m), and the above-0.5 V capacities range from 226 mAh g^{-1} (0.5 m) to 289 mAh g^{-1} (4.0 m). Interestingly, the *dQ/dV* peak broadens with increasing salt concentration, and the above-0.5 V capacity is largest for the 4.0 m experiment. The latter result is unexpected given that the EC concentration decreases with salt concentration; we generally expect larger reduction capacities for larger reactant concentrations. One speculative hypothesis for this result is that EC reduction is more facile at higher salt concentrations because the EC is bound less tightly in the lithium-ion solvation shell as the lithium ions become solvated by PF_6^- anions,[84] and this effect increases capacity loss more than the decreased EC concentration decreases capacity loss.

We find that the peak potential decreases linearly with salt concentration, i.e. decreasing EC concentration (Fig. 5d). This result is consistent with the expected reaction order (i.e., the overpotential is minimized when the reactant is most abundant), but the degree of linearity is surprising given the diversity of solvation structures that appear throughout this concentration range.[83–85] We note that unlike the C rate and temperature experiments, the irreversible capacity loss does not change substantially with peak potential, and in fact is inversely correlated with peak potential (irreversible capacity loss is directly correlated with peak potential for the C rate and temperature experiments). Overall, the irreversible capacity loss from first-cycle EC reduction is much less sensitive to salt concentration than to

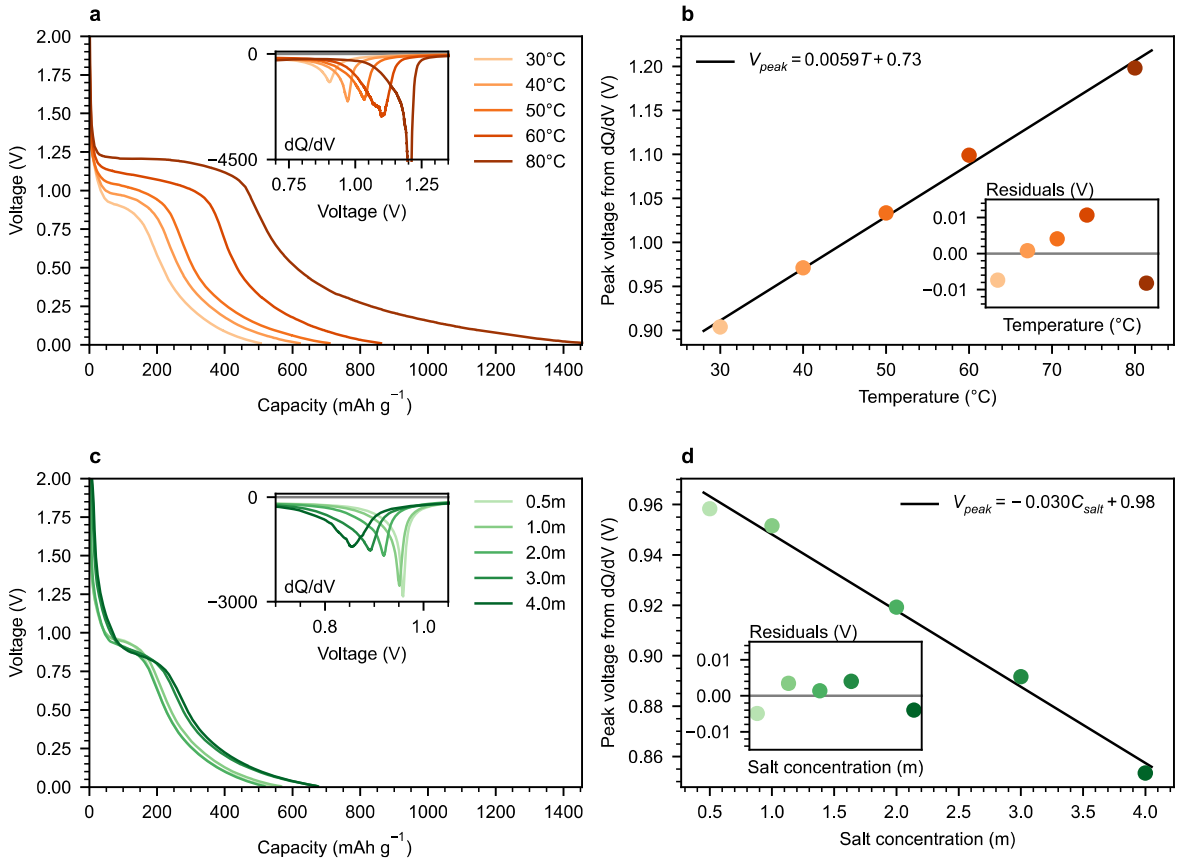

Figure 5. Dependence of the EC reduction reaction on temperature and salt concentration. (a) Voltage vs capacity and (b) peak voltage vs temperature is displayed for five values of temperature. Both peak potential and irreversible capacity loss increase with increasing temperature. (c) Voltage vs capacity and (d) peak voltage vs salt concentration is displayed for five values of salt concentration. Peak potential decreases, and irreversible capacity loss (slightly) increases, with increasing salt concentration. Differential capacity (*dQ/dV*, units of mAh g^{-1} V^{-1}) vs voltage is displayed in the insets of panels (a) and (c), and the residuals of linear fits are displayed in the insets of panels (b) and (d). All cells cycle at a nominal rate of C/10.

temperature. Combined with the less practical nature of controlling salt concentration during formation, we primarily focus on the C rate and temperature dependences in the following discussion.

Discussion

Our results paint a simplified picture of the first-cycle EC reduction reaction that can explain both the results shown here and those of previous literature. Previous work has established that EC in the lithium-ion solvation shell can cointercalate into and exfoliate the carbonaceous non-basal-plane surfaces, becoming reduced in the process.[9,10,21,23–25] This reaction consumes large amounts of lithium inventory. In this work, we established that the cyclic carbonate reduction products provide no passivation ability (Figs. 2 and 3). Thus, the effects of EC reduction (as defined in this work, i.e., "EC reduction above 0.5 V during the first lithiation") are entirely detrimental: it consumes lithium inventory, increases the formation time, generates gas (which can cause swelling in pouch cells[87,88]), and fails to passivate the electrode. In short, the EC reduction reaction should be minimized as much as possible. Fortunately, this reaction ceases once the low-potential passivating reactions begin.

Our results illustrate two primary approaches for decreasing the irreversible capacity loss from EC reduction: high applied currents and low temperatures. We posit that the explanation for these observations can be deduced from fundamental electrochemical principles, as opposed to being a unique feature of this system. To begin, we discuss the two concurrent processes during the first cycle. Lithiation is, of course, a standard reaction in modern batteries, and its capacity is constrained by the smaller of (a) the available lithium inventory in the cell or (b) the capacity of the delithiated electrode material. In contrast, EC reduction is analogous to many classical electrochemical systems: the electrolyte solution is both the reactant source and product sink. Since the EC reduction products do not effectively passivate the electrode, the maximum capacity of EC reduction is limited only by the availability of EC in the electrolyte and lithium ions in the counter electrode for cells with flooded electrodes (including the cells used in this work); however, this capacity may be constrained in commercial cells with lower ratios of electrolyte volume to electrode mass. In the rest of this discussion, we distinguish between "host-constrained" reactions and "host-unconstrained" reactions, the most relevant difference between them being the presence of a capacity-constraining host material. Both types of reactions can be assumed to have an infinite reservoir of all reactants (except vacancies in the host material for host-constrained reactions, which is technically a reactant for host-constrained reactions). Because lithiation and EC reduction are independent destinations for the electronic current, these two processes can be thought of as two branches in a parallel circuit.

To further study this system, we perform linear sweep voltammetry (LSV) at variable sweep rates for the first lithiation of carbon black (Fig. 6). LSV is a useful probe for parallel processes because the current responses of the processes to changes from the externally-controlled voltage are independent. Additionally, the fundamental scaling relationships between variables such as current, potential, and sweep rate are well established.[82] Although the control technique certainly can influence the SEI kinetics,[66,67] we note that the voltage vs capacity curves from both LSV and galvanostatic cycling are similar (Fig. 6c), which eases the comparison between the two methods.

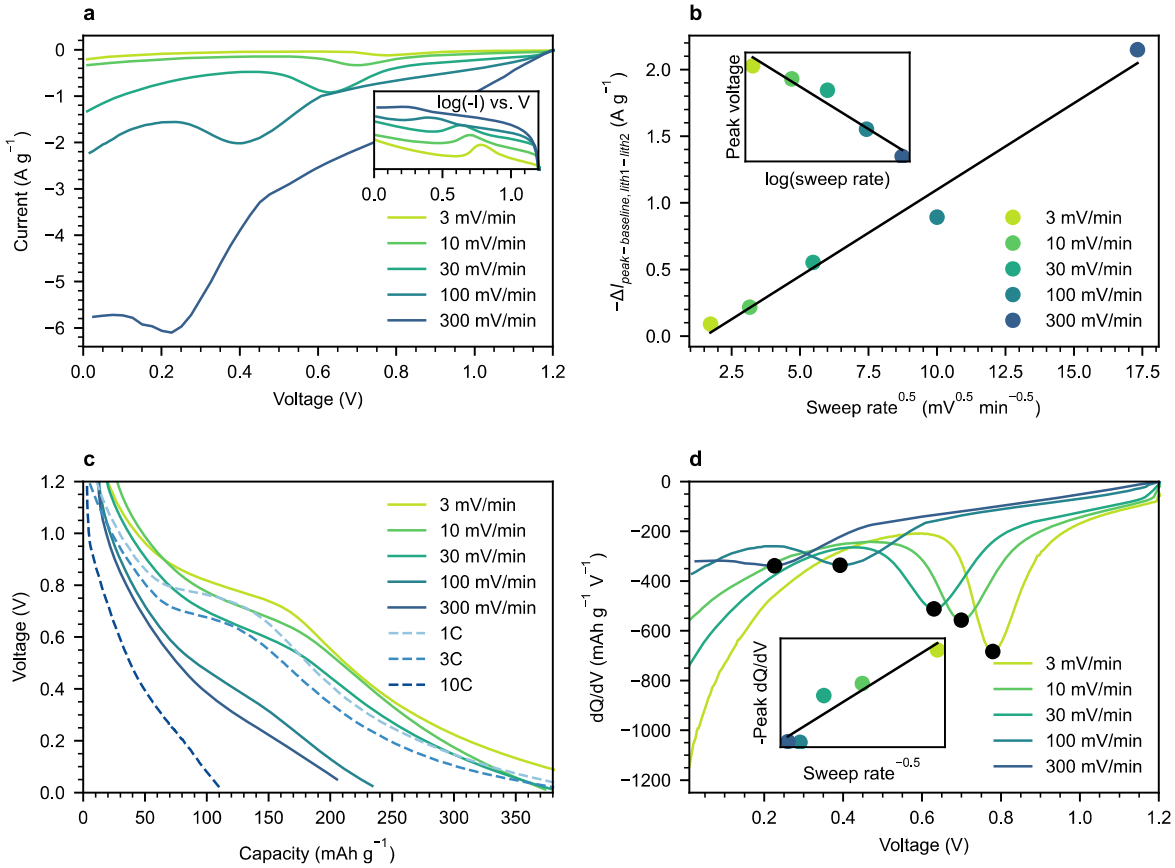

Figure 6. Linear sweep voltammetry (LSV) of the first lithiation of carbon black as a function of sweep rate. (a) Current vs voltage as a function of sweep rate. The logarithm of negative current vs voltage is displayed in the inset. (b) Baseline-corrected peak $-\Delta I_{lith1-lith2}$ ($-\Delta I_{peak-baseline,lith1-lith2}$) vs the square root of sweep rate. The trend is linear, possibly indicating a diffusion limitation. The derivation of $-\Delta I_{peak-baseline,lith1-lith2}$ is presented in Fig. S3. The peak potential vs the logarithm of sweep rate is displayed in the inset; this trend is also linear, indicating electrochemically irreversible behavior. (c) Voltage vs capacity from the first lithiation of carbon black via both galvanostatic cycling and LSV, as a function of C rate and sweep rate. While the qualitative trends between this experiment and the galvanostatic experiment are similar, the EC reduction peak is still present at low potentials for the LSV experiments, even at high sweep rates. (d) *dQ/dV* vs voltage for the LSV experiments; in LSV, *dQ/dV* is equivalent to current divided by sweep rate. The negative of the peak *dQ/dV* values vs the inverse square root of the sweep rate are displayed in the inset. While the magnitude of the peak current increases with sweep rate, the magnitude of the peak capacity decreases with sweep rate. Note that because the electrode masses were unavailable for the LSV experiments, a nominal mass of 0.8 mg is used for all cells.

Figure 6a presents current vs voltage during LSV for five sweep rates ranging from 3 mV min^{-1} (0.05 mV s^{-1}) to 300 mV min^{-1} (5 mV s^{-1}). Current peaks corresponding to EC reduction are observed at similar potentials to the *dQ/dV* peaks in galvanostatic cycling. In LSV, a current peak often corresponds to a transition from a reaction limitation to a diffusion limitation. This transition is observed as long as the sweep reaches potentials much more extreme than the equilibrium redox potential; since the reaction kinetics scale exponentially with overpotential (i.e., the Butler-Volmer equation), the current will eventually be limited by reactant availability at extreme potentials. In this case, the limiting reaction corresponds to EC reduction, while the limiting diffusion species is presumably $Li^+(EC)_4$ in the electrolyte.

Again, while EC reduction is diffusion limited at all sweep rates and currents used in this investigation, carbon black lithiation is only diffusion limited for currents at the higher end of this range (above ~C/5).[66] One factor that contributes to EC reduction becoming transport limited at lower rates than carbon lithiation is that the equilibrium potential of EC reduction ($\gg$1.05 V, as discussed previously) is ~1 V higher than the potentials at which most carbon black lithiation occurs (~0–0.2 V). Thus, the overpotential for EC reduction is much higher than that of carbon lithiation throughout the formation cycle. However, other factors such as the exchange current densities and the diffusivities also define the relative transport limitations of these processes.

In Fig. 6b, we estimate the peak currents corresponding to EC reduction. We subtract the current of the second lithiation from that of the first lithiation, and then subtract a baseline value corresponding to the start of the EC reduction peak (Fig. S3). We find that the baseline-corrected peak currents approximately scale with the square root of the sweep rate. Peak current scaling with the square root of the sweep rate often suggests a diffusion-limited process; the Randles–Sevcik equation is one well-known relationship demonstrating this scaling.[82] We note that the square root scaling of peak current on scan rate can also arise from other types of limitations (e.g., ohmic),[89] but we assume this reaction is diffusion-limited throughout the rest of this discussion. We estimated the diffusivity of this reaction using a variant of the Randles–Sevcik equation suitable for electrochemically irreversible processes (Fig. S4 and Supplementary Discussion 1), although we acknowledge some limitations in its applicability (e.g., the presence of a subsequent chemical reaction in this system).[82] Our estimates yield $D_{Li+(EC)4} \approx 10^{-19}$ m^2 s^{-1}, which is 9–10 orders of magnitude below literature estimates of bulk EC diffusivity in this electrolyte system (10^{-9}–10^{-10} m^2 s^{-1})[90,91] and 0–10 orders of magnitude below literature estimates of bulk lithium-ion diffusivity in graphite (in-plane diffusivity of 10^{-10}–10^{-11} m^2 s^{-1})[92] and lithium iron phosphate (10^{-20}–10^{-10} m^2 s^{-1}; wide range of values reported).[93–95] This diffusivity is also three orders of magnitude lower than the estimated diffusivity of lithium on the surface of

lithium iron phosphate ($>10^{-16}$ m^2 s^{-1}),[96] but at least closer; perhaps solvent co-intercalation (i.e., insertion of a bulky solvation complex at edge planes) is a surface-diffusion-limited process. Both the interpretation of this value and identification of a more suitable estimation method are under further investigation.

The peak potential decreases roughly with the logarithm of sweep rate (inset of Fig. 6b). This relationship confirms that this reaction is electrochemically irreversible (i.e., slow reaction kinetics relative to sweep rate)[82] at the sweep rates used here, which have similar time scales to the high-current galvanostatic experiments.

Figures 6c–6d present useful, albeit unconventional, analysis of LSV. In Fig. 6c, we compute a running integral of the current to obtain voltage vs capacity. For comparison, we overlay the traces from the three fastest one-step formations from Fig. 2b. In general, voltage vs capacity for the LSV experiments closely resemble that of the galvanostatic experiments. Note that the EC reduction peak is (slightly) visible for the 300 mV min^{-1} experiment, even though this peak is suppressed for the 10C experiment; we return to this point shortly. In Fig. 6d, we display dQ/dV vs voltage for the LSV experiments; in LSV, dQ/dV is equivalent to the current divided by the sweep rate. The inset displays the peak dQ/dV value as a function of the inverse square root of the sweep rate. Overall, we find that the largest EC reduction capacities are obtained with the slowest sweep rates. This result may seem counterintuitive: while the EC reduction *current* increases with sweep rate, the EC reduction *capacity* decreases with sweep rate. In fact, this feature is fundamental to "host-unconstrained" reactions with high reactant supply investigated via LSV at low sweep rates. As previously discussed, the peak current scales with the square root of sweep rate. However, for a fixed voltage window (such as in sweep voltammetry), the time scales with the inverse of sweep rate. Thus, since capacity is the integral of current with respect to time, the capacity scales with the inverse square root of the sweep rate for host-unconstrained systems with high reactant supply. As a result, the total capacity lost to EC reduction decreases with sweep rate. Note that this scaling only holds at sweep rates (and currents in galvanostatic cycling) for which a peak current is observed; at higher sweep rates, the system may not reach the diffusion-limited regime. In summary, because EC reduction becomes limited by diffusion before carbon lithiation, the EC reduction capacity decreases more quickly than the lithiation capacity as the sweep rate increases.

This principle generally applies during galvanostatic operation as well. However, galvanostatic operation has two important differences from LSV operation. First, the capacity of host-unconstrained reactions with high reactant supply theoretically scales with the inverse of current in galvanostatic operation, as opposed to the inverse square root of current as in LSV. Again, capacity is the integral of current with respect to time, or simply the product of current and time if the current is constant. However, the characteristic time of host-unconstrained systems under galvanostatic control, or Sand's time, scales with the inverse square of current.[82] Thus, capacity is expected to scale with the inverse of current. This scaling differs from that of host-constrained processes like carbon black (de)lithiation, where diffusion is not limiting at moderate current densities; as a result, the capacity is only weakly dependent on current. The stronger sensitivity of diffusion-limited reactions to current can be leveraged for additional suppression of EC reduction by simply applying a high current. We note that our observed scaling of the EC reduction capacity with applied current is weaker than the linear inverse (Fig. 3c), which we attribute to the effect of the competing lithiation current on time (Fig. 2e).

The second difference between galvanostatic and LSV operation is that the total current is constrained in galvanostatic cycling. The effects of this constraint are most pronounced for high-surface-area electrodes such as carbon black and are only a weak contributor for low-surface-area electrodes such as commercially-relevant graphite electrodes; while this effect plays only a minor role for commercially relevant formation processes, we discuss this effect here for completeness. Our incomplete understanding of the EC reduction sequence notwithstanding, we can broadly say that EC reduction and carbon black lithiation are concurrent processes during part of the first cycle. During galvanostatic cycling, these processes compete for the fixed current, analogous to two parallel branches of a circuit. If EC reduction is promoted relative to lithiation, the electrode potential changes slowly, and large amounts of irreversible capacity loss occurs due to EC reduction. In contrast, if lithiation obtains most of the current, the potential will rapidly decrease, and the lithiating electrode will begin to form the low-potential reduction products that do provide passivation, which prevent EC reduction on subsequent cycles (Fig. 2f).

However, lithiation has a significant disadvantage in its competition with EC reduction for current: lithiation is host-constrained, while EC reduction is host-unconstrained. Thus, if left unchecked (i.e., cycled at low rates), EC reduction can cause massive irreversible capacity loss without appreciable lithiation. Fortunately, we can also exploit this "current competition" to suppress EC reduction via galvanostatic cycling at high rates. To see this effect clearly, note that the EC reduction peak is observed at low potential in the 300 mV min^{-1} LSV experiment, but not during the 10C galvanostatic experiment. In the latter case, lithiation effectively competes for current at these potentials because EC reduction becomes diffusion-limited more readily than carbon lithiation. While some EC reduction is unavoidable, its detrimental effects can be readily mitigated by the use of high current during galvanostatic cycling.

We proposed a similar mechanism of current competition between lithiation and SEI growth in our previous work on "post-first-cycle" SEI growth on carbon black.[66] In those experiments, we found a similar result: while the irreversible capacity loss scaled with the inverse of the applied current, the *rate* of irreversible capacity loss increased linearly with the applied current. We suspect that a similar mechanism applies broadly to the general case of electrochemical systems with a charge storage reservoir and associated unconstrained side reactions (i.e., coupled host-constrained and host-unconstrained reactions) under galvanostatic control. Again, this effect is important for high-surface-area systems with large side reaction rates and high reactant concentrations (e.g., electrodes with high carbon black content) but only plays a small role for electrodes with lower surface area (e.g., most commercially relevant graphitic electrodes).

Building on these insights, we now turn towards the temperature results. Similar principles apply here as well to explain how high temperatures promote EC reduction. Increased temperature improves the kinetics of both lithiation and EC reduction, but because the lithiation capacity is constrained and the EC reduction capacity is unconstrained, EC reduction consumes massive amounts of capacity at high temperature (see Fig. 4a, 80 °C). Conversely, less capacity is consumed by EC reduction at lower temperatures. Thus, an efficient formation protocol can be obtained via a combination of high currents and low temperatures, provided other degradation modes promoted by these conditions (e.g., lithium plating) are avoided. We also propose that large quantities of EC reduction products can be easily generated for scientific purposes (e.g., compositional analysis[37]) by cycling at low rates and high temperatures.

This simple mechanism has interesting implications when revisiting the EC/PC controversy that held back the commercialization of lithium-ion batteries for decades.[10,21,22,59] PC perpetually reduces at moderate rates and temperatures, not unlike EC at low rates and high temperatures. The molecular-level understanding of what exactly leads to these dramatic differences is still not entirely clear, and beyond the scope of this work, though recent progress has been made[27,59] (as an aside, we mention that a similar solvation-related "magic methyl" effect has been observed in drug development[97]). However, we can phenomenologically summarize these differences by saying the reduction kinetics (typically

measured by the standard heterogeneous rate constant of reduction, k^0) are higher for PC than EC, as evidenced by the large irreversible capacity loss of PC relative to EC under similar conditions.[10,45] Despite PC's intrinsically higher propensity to reduce, our results and interpretation provide pathways that could favor reversible lithiation from PC electrolytes over indefinite reduction: high currents and low temperatures. Indeed, reversible lithiation into graphite from PC electrolytes has been previously demonstrated under those exact conditions: high rates[98] (>5C) and low temperatures[99] (<−15 °C)! We note that reversible lithiation into graphite from PC electrolytes has also been observed at high salt concentrations (∼3 M).[24,26]

A similar argument could explain why the common cyclic carbonate additives VC and FEC have low irreversible capacity loss and gas generation during the first cycle:[8,10,50,52,53] poor reduction kinetics (i.e., low k^0). In fact, Peled[100] reported a correlation between k_{e^-}, the aqueous rate constant for the reduction of electrolyte components by hydrated electrons (a previously tabulated measurement), and the peak dQ/dV reduction potential on graphite. While the benefit of these additives in formation is often attributed to the passivating properties of their reduction products (e.g., low porosity, high elasticity), our work demonstrates that lithium can intercalate into graphitic carbons from EC-based electrolytes even though the EC reduction products do not provide any passivation ability. Thus, we hypothesize that the morphological properties of the additive reduction products do not substantially aid in passivation, especially during low-rate cycling when mass transport is not limiting; instead, these additives reduce less easily than EC and thus have less irreversible capacity loss during formation. Broadly speaking, we expect that the use of high currents and low temperatures during formation could enable new electrolyte salts, solvents, and additives that may have been previously assumed to have prohibitively large irreversible first-cycle capacity fade, although this design rule ignores potential complications at the positive electrode.

An important difference worth revisiting is that of graphite and carbon black. As previously discussed, graphite powders used in batteries generally have much lower specific surface areas than carbon black, which decreases the observed irreversible capacity loss. In general, the capacity loss from EC reduction on graphite is small (Fig. 1a). Additionally, graphite has another advantage over carbon black in terms of minimizing EC reduction: the voltage curve is steeper (dQ/dV between 0.5 V and 1.0 V is 13× larger in carbon black than graphite). Thus, during galvanostatic cycling at high rates, graphite lithiation will rapidly decrease the potential to the regime in which EC reduction ceases. In short, the steep voltage curve at the potentials of EC reduction is a fortunate property of graphite. Overall, EC reduction does not consume nearly as much capacity during formation for cells with graphite negative electrodes compared to carbon black negative electrodes, but this work highlights an opportunity to decrease both formation time and first-cycle capacity loss without impacting lifetime for any cell with a carbonaceous negative electrode.

Finally, we consider strategies for quickly growing well-passivating low-potential SEI during formation. The low-potential SEI formed during the first lithiation has similar characteristics to the "post-first-cycle" low-potential SEI studied in our previous work.[66] In this work, we identified that the SEI growth rate is exponential with decreasing negative electrode potential and linear with increasing applied C rate. Thus, a formation cycling protocol that minimizes formation time and subsequent-cycle capacity loss is relatively rapid, shallow cycling at high cell potentials, similar to the C/5a ("alternative") formation protocol proposed by An et al.[13] for NMC/graphite cells or the 10C(0.5 V)-1C protocol proposed in the discussion of Fig. 4 in this work. The combination of high rates and cell potentials (while avoiding major transport limitations and lithium plating) drives the growth of well-passivating SEI while minimizing the growth of poorly passivating SEI. Performing the shallow high-potential cycling at high temperatures would also accelerate the growth of beneficial SEI during formation. Overall, these principles suggest that formation should occur at the highest rate possible while avoiding both major transport limitations and lithium plating.

In summary, we propose a strategy to increase Coulombic efficiency during the first cycle. With essentially no limitations on how much EC reduction can occur, this diffusion-limited process can lead to massive irreversible capacity loss at low rates. However, the capacity of lithiation is not diffusion-limited at typical current densities. As a result, both high sweep rates and high applied currents suppress the irreversible capacity loss from EC reduction while still allowing for intercalation. Following similar logic, low temperatures also suppress the kinetics of EC reduction and thus decrease the irreversible capacity loss. In short, these pathways towards minimizing the reduction of cyclic carbonates during the first cycle could unlock both improved formation protocols and new classes of battery electrolytes.

Conclusions

In this work, we present systematic studies of the EC reduction kinetics during formation of carbon black. We first compare the first few cycles of graphite and carbon black; the EC reduction reaction occurring at ∼0.6–1.1 V is generally confined to the first lithiation, making it a distinct reaction from subsequent-cycle SEI growth and even low-potential first-lithiation SEI growth. Our simple electrochemical experiments demonstrate that while the EC reduction reaction leads to major irreversible capacity loss and increases the formation time, its products provide no passivation (as measured by second-cycle Coulombic efficiency). Fortunately, high formation currents decrease both formation time and formation capacity loss from EC reduction—welcome news for battery manufacturing. We also demonstrate how the irreversible capacity loss of the EC reduction reaction increases with temperature and salt concentration, with temperature being an especially sensitive parameter. Finally, we propose a simple phenomenological scheme that explains how to suppress EC reduction and (possibly) unlock new electrolytes that were previously assumed to have prohibitively large irreversible first-cycle capacity fade.

Optimized formation processes balance time, first-cycle losses, subsequent-cycle losses, and impedance. Our work illustrates and quantifies the tradeoffs between these parameters using carbon black as a model system. We expect that the principles outlined here should generalize to other carbonaceous negative electrodes with a cyclic carbonate cosolvent. Nonetheless, we recognize that our model system differs substantially from a commercial cell. Future formation optimization work should consider the additional complications from incorporating graphitic negative electrodes, full cells with relevant positive electrode materials, modern electrolytes with state-of-the-art additives, lower ratios of electrolyte volume to electrode capacity, and other aspects of formation such as wetting and defect detection. Furthermore, optimization of the formation protocol at low negative electrode potentials can likely lead to additional improvements. Finally, the sensitivity of long-term capacity loss and impedance growth to formation should be evaluated in full cells. As a whole, these results provide insights towards optimizing formation cycling and electrolyte design in commercial lithium-ion batteries and thus improving their energy density, lifetime, and cost.

Acknowledgments

This work is funded by Vehicle Technologies Office of the US Department of Energy under the Extreme Fast Charging program and by the Toyota Research Institute through the Accelerated Materials Design and Discovery program. P.M.A. was supported

by the Thomas V. Jones Stanford Graduate Fellowship and the National Science Foundation Graduate Research Fellowship under grant No. DGE-1656518. S.J.H. was supported by the Assistant Secretary for Energy Efficiency, Vehicle Technologies Office of the US Department of Energy under the Advanced Battery Materials Research program. We thank Peter Csernica, Xiao Cui, Supratim Das, Norman Jin, Stephen Kang, Tyler Mefford, Henry Thaman, and Che-Ning Yeh for insightful discussions.

Data Availability

All data and code are publicly available in the associated Zenodo repository[101] and on GitHub (https://www.github.com/petermattia/first-cycle-SEI-on-carbon-black).

ORCID

Peter M. Attia https://orcid.org/0000-0003-4745-5726
Stephen J. Harris https://orcid.org/0000-0002-5211-3934
William C. Chueh https://orcid.org/0000-0002-7066-3470

References

1. B. Nykvist and M. Nilsson, *Nat. Clim. Change*, **5**, 329 (2015).
2. S. Chu, Y. Cui, and N. Liu, *Nat. Mater.*, **16**, 16 (2017).
3. Z. P. Cano, D. Banham, S. Ye, A. Hintennach, J. Lu, M. Fowler, and Z. Chen, *Nat. Energy*, **3**, 279 (2018).
4. V. A. Agubra and J. W. Fergus, *J. Power Sources*, **268**, 153 (2014).
5. D. L. Wood, J. Li, and C. Daniel, *J. Power Sources*, **275**, 234 (2015).
6. S. J. An, J. Li, C. Daniel, D. Mohanty, S. Nagpure, and D. L. Wood, *Carbon*, **105**, 52 (2016).
7. D. L. Wood, J. Li, and S. J. An, *Joule*, **3**, 2884 (2019).
8. K. Xu, *Chem. Rev.*, **104**, 4303 (2004).
9. P. Verma, P. Maire, and P. Novák, *Electrochim. Acta*, **55**, 6332 (2010).
10. K. Xu, *Chem. Rev.*, **114**, 11503 (2014).
11. E. Peled and S. Menkin, *J. Electrochem. Soc.*, **164**, A1703 (2017).
12. P.-C. J. Chiang, M.-S. Wu, and J.-C. Lin, *Electrochem. Solid-State Lett.*, **8**, A423 (2005).
13. S. J. An, J. Li, Z. Du, C. Daniel, and D. L. Wood, *J. Power Sources*, **342**, 846 (2017).
14. V. Müller, R. Kaiser, S. Poller, D. Sauerteig, R. Schwarz, M. Wenger, V. R. H. Lorentz, and M. März, *J. Energy Storage*, **14**, 56 (2017).
15. V. Müller, R. Kaiser, S. Poller, and D. Sauerteig, *J. Energy Storage*, **15**, 256 (2018).
16. C. Mao, S. J. An, H. M. Meyer, J. Li, M. Wood, R. E. Ruther, and D. L. Wood, *J. Power Sources*, **402**, 107 (2018).
17. B. K. Antonopoulos, F. Maglia, F. Schmidt-Stein, J. P. Schmidt, and H. E. Hoster, *Batter. Supercaps*, **1**, 110 (2018).
18. B. K. Antonopoulos, C. Stock, F. Maglia, and H. E. Hoster, *Electrochim. Acta*, **269**, 331 (2018).
19. T. S. Pathan, M. Rashid, M. Walker, W. D. Widanage, and E. Kendrick, *J. Phys.: Energy*, **1**, 044003 (2019).
20. A. Moretti, V. Sharova, D. V. Carvalho, A. Boulineau, W. Porcher, I. de Meatza, and S. Passerini, *Batter. Supercaps*, **2**, 240 (2019).
21. M. Winter, B. Barnett, and K. Xu, *Chem. Rev.*, **118**, 11433 (2018).
22. A. N. Dey and B. P. Sullivan, *J. Electrochem. Soc.*, **117**, 222 (1970).
23. J. O. Besenhard, M. Winter, J. Yang, and W. Biberacher, *J. Power Sources*, **54**, 228 (1995).
24. S.-K. Jeong, M. Inaba, Y. Iriyama, T. Abe, and Z. Ogumi, *Electrochem. Solid-State Lett.*, **6**, A13 (2003).
25. M. R. Wagner, J. H. Albering, K.-C. Moeller, J. O. Besenhard, and M. Winter, *Electrochem. Commun.*, **7**, 947 (2005).
26. M. Nie, D. P. Abraham, D. M. Seo, Y. Chen, A. Bose, and B. L. Lucht, *J. Phys. Chem. C*, **117**, 25381 (2013).
27. I. A. Shkrob, Y. Zhu, T. W. Marin, and D. Abraham, *J. Phys. Chem. C*, **117**, 19255 (2013).
28. R. Fong, U. von Sacken, and J. R. Dahn, *J. Electrochem. Soc.*, **137**, 2009 (1990).
29. M. Winter and J. O. Besenhard, *Lithium Ion Batteries: Fundamentals and Performance*, ed. M. Wakihara and O. Yamamoto (Wiley-VCH Verlag GmbH, Weinheim, Germany) p. 127 (1998).
30. V. Etacheri, R. Marom, R. Elazari, G. Salitra, and D. Aurbach, *Energy Environ. Sci.*, **4**, 3243 (2011).
31. M. E. Spahr, T. Palladino, H. Wilhelm, A. Würsig, D. Goers, H. Buqa, M. Holzapfel, and P. Novák, *J. Electrochem. Soc.*, **151**, A1383 (2004).
32. M. E. Spahr, H. Buqa, A. Würsig, D. Goers, L. Hardwick, P. Novák, F. Krumeich, J. Dentzer, and C. Vix-Guterl, *J. Power Sources*, **153**, 300 (2006).
33. M. E. Spahr, D. Goers, W. Märkle, J. Dentzer, A. Würsig, H. Buqa, C. Vix-Guterl, and P. Novák, *Electrochim. Acta*, **55**, 8928 (2010).
34. R. Bernhard, M. Metzger, and H. A. Gasteiger, *J. Electrochem. Soc.*, **162**, A1984 (2015).
35. G. V. Zhuang, K. Xu, H. Yang, T. R. Jow, and P. N. Ross, *J. Phys. Chem. B*, **109**, 17567 (2005).
36. M. Nie, D. Chalasani, D. P. Abraham, Y. Chen, A. Bose, and B. L. Lucht, *J. Phys. Chem. C*, **117**, 1257 (2013).
37. L. Wang et al., *Nat. Chem.*, **11**, 789 (2019).
38. J. P. Olivier and M. Winter, *J. Power Sources*, **97–98**, 151 (2001).
39. T. Placke, V. Siozios, R. Schmitz, S. F. Lux, P. Bieker, C. Colle, H.-W. Meyer, S. Passerini, and M. Winter, *J. Power Sources*, **200**, 83 (2012).
40. T. Placke, V. Siozios, S. Rothermel, P. Meister, C. Colle, and M. Winter, *Z. Für Phys. Chem.*, **229**, 1451 (2015).
41. K. Xu, *J. Electrochem. Soc.*, **154**, A162 (2007).
42. K. Xu, Y. Lam, S. S. Zhang, T. R. Jow, and T. B. Curtis, *J. Phys. Chem. C*, **111**, 7411 (2007).
43. K. Xu and A. von Cresce, *J. Mater. Chem.*, **21**, 9849 (2011).
44. A. von Cresce and K. Xu, *Electrochem. Solid State Lett.*, **14**, A154 (2011).
45. A. von Wald Cresce, O. Borodin, and K. Xu, *J. Phys. Chem. C*, **116**, 26111 (2012).
46. K. A. See, M. A. Lumley, G. D. Stucky, C. P. Grey, and R. Seshadri, *J. Electrochem. Soc.*, **164**, A327 (2017).
47. W. Märkle, C.-Y. Lu, and P. Novák, *J. Electrochem. Soc.*, **158**, A1478 (2011).
48. W. Huang et al., *Nano Lett.*, **19**, 5140 (2019).
49. M. E. Spahr, H. Wilhelm, F. Joho, J.-C. Panitz, J. Wambach, P. Novák, and N. Dupont-Pavlovsky, *J. Electrochem. Soc.*, **149**, A960 (2002).
50. R. McMillan, H. Slegr, Z. X. Shu, and W. Wang, *J. Power Sources*, **81–82**, 20 (1999).
51. Y. Wang, S. Nakamura, K. Tasaki, and P. B. Balbuena, *J. Am. Chem. Soc.*, **124**, 4408 (2002).
52. D. Aurbach, K. Gamolsky, B. Markovsky, Y. Gofer, M. Schmidt, and U. Heider, *Electrochim. Acta*, **47**, 1423 (2002).
53. L. E. Ouatani, R. Dedryvère, C. Siret, P. Biensan, and D. Gonbeau, *J. Electrochem. Soc.*, **156**, A468 (2009).
54. T. Li and P. B. Balbuena, *Chem. Phys. Lett.*, **317**, 421 (2000).
55. Y. Wang, S. Nakamura, M. Ue, and P. B. Balbuena, *J. Am. Chem. Soc.*, **123**, 11708 (2001).
56. A. Wang, S. Kadam, H. Li, S. Shi, and Y. Qi, *NPJ Comput. Mater.*, **4**, 15 (2018).
57. K. Leung, *Chem. Phys. Lett.*, **568–569**, 1 (2013).
58. J. M. Reniers, G. Mulder, and D. A. Howey, *J. Electrochem. Soc.*, **166**, A3189 (2019).
59. L. Xing, X. Zheng, M. Schroeder, J. Alvarado, A. von Wald Cresce, K. Xu, Q. Li, and W. Li, *Acc. Chem. Res.*, **51**, 282 (2018).
60. T. Liu et al., *Nat. Nanotechnol.*, **14**, 50 (2019).
61. D. Goers, M. E. Spahr, A. Leone, W. Märkle, and P. Novák, *Electrochim. Acta*, **56**, 3799 (2011).
62. S. Zhang, M. S. Ding, K. Xu, J. Allen, and T. R. Jow, *Electrochem. Solid-State Lett.*, **4**, A206 (2001).
63. K. Edström, M. Herstedt, and D. P. Abraham, *J. Power Sources*, **153**, 380 (2006).
64. P. Lu and S. J. Harris, *Electrochem. Commun.*, **13**, 1035 (2011).
65. P. Lu, C. Li, E. W. Schneider, and S. J. Harris, *J. Phys. Chem. C*, **118**, 896 (2014).
66. P. M. Attia, S. Das, S. J. Harris, M. Z. Bazant, and W. C. Chueh, *J. Electrochem. Soc.*, **166**, E97 (2019).
67. S. Das, P. M. Attia, W. C. Chueh, and M. Z. Bazant, *J. Electrochem. Soc.*, **166**, E107 (2019).
68. J. R. Dahn, T. Zheng, Y. Liu, and J. S. Xue, *Science*, **270**, 590 (1995).
69. A. K. Sleigh and U. von Sacken, *Solid State Ion.*, **57**, 99 (1992).
70. K. Takei, N. Terada, K. Kumai, T. Iwahori, T. Uwai, and T. Miura, *J. Power Sources*, **55**, 191 (1995).
71. R. Yazami and M. Deschamps, *J. Power Sources*, **54**, 411 (1995).
72. L. Fransson, T. Eriksson, K. Edström, T. Gustafsson, and J. O. Thomas, *J. Power Sources*, **101**, 1 (2001).
73. A. J. Smith, J. C. Burns, X. Zhao, D. Xiong, and J. R. Dahn, *J. Electrochem. Soc.*, **158**, A447 (2011).
74. A. L. Michan, M. Leskes, and C. P. Grey, *Chem. Mater.*, **28**, 385 (2016).
75. J.-B. Donnet, R. C. Bansal, and M.-J. Wang (ed.), *Carbon black: Science and Technology* (Dekker, New York, NY) 2nd ed. (1993).
76. K. Kinoshita, *Carbon: Electrochemical and Physicochemical Properties* (Wiley, New York, NY) (1988).
77. P. M. Attia, W. C. Chueh, and S. J. Harris, *J. Electrochem. Soc.*, **167**, 090535 (2020).
78. J. C. Burns, A. Kassam, N. N. Sinha, L. E. Downie, L. Solnickova, B. M. Way, and J. R. Dahn, *J. Electrochem. Soc.*, **160**, A1451 (2013).
79. D. Aurbach, B. Markovsky, I. Weissman, E. Levi, and Y. Ein-Eli, *Electrochim. Acta*, **45**, 67 (1999).
80. D. Aurbach, E. Zinigrad, Y. Cohen, and H. Teller, *Solid State Ion.*, **148**, 405 (2002).
81. J. Ming et al., *ACS Energy Lett.*, **3**, 335 (2018).
82. A. J. Bard and L. R. Faulkner, *Electrochemical Methods: Fundamentals and Applications* (Wiley, New York, NY) 2nd ed., p. 833 (2001).
83. Y. Yamada, J. Wang, S. Ko, E. Watanabe, and A. Yamada, *Nat. Energy*, **4**, 269 (2019).
84. Y. Yamada and A. Yamada, *J. Electrochem. Soc.*, **162**, A2406 (2015).
85. O. Borodin, J. Self, K. A. Persson, C. Wang, and K. Xu, *Joule*, **4**, 69 (2020).
86. L. O. Valøen and J. N. Reimers, *J. Electrochem. Soc.*, **152**, A882 (2005).
87. C. P. Aiken, J. Self, R. Petibon, X. Xia, J. M. Paulsen, and J. R. Dahn, *J. Electrochem. Soc.*, **162**, A760 (2015).

88. J. Self, C. P. Aiken, R. Petibon, and J. R. Dahn, *J. Electrochem. Soc.*, **162**, A796 (2015).
89. A. J. Calandra, N. R. de Tacconi, R. Pereiro, and A. J. Arvia, *Electrochim. Acta*, **19**, 901 (1974).
90. K. Hayamizu, *J. Chem. Eng. Data*, **57**, 2012 (2012).
91. Z. Feng, K. Higa, K. S. Han, and V. Srinivasan, *J. Electrochem. Soc.*, **164**, A2434 (2017).
92. K. Persson, V. A. Sethuraman, L. J. Hardwick, Y. Hinuma, Y. S. Meng, A. van der Ven, V. Srinivasan, R. Kostecki, and G. Ceder, *J. Phys. Chem. Lett.*, **1**, 1176 (2010).
93. P. P. Prosini, M. Lisi, D. Zane, and M. Pasquali, *Solid State Ion.*, **148**, 45 (2002).
94. H. Liu, C. Li, H. P. Zhang, L. J. Fu, Y. P. Wu, and H. Q. Wu, *J. Power Sources*, **159**, 717 (2006).
95. R. Malik, D. Burch, M. Bazant, and G. Ceder, *Nano Lett.*, **10**, 4123 (2010).
96. Y. Li et al., *Nat. Mater.*, **17**, 915 (2018).
97. H. Schönherr and T. Cernak, *Angew. Chem. Int. Ed.*, **52**, 12256 (2013).
98. H.-Y. Song and S.-K. Jeong, *J. Anal. Methods Chem.*, **2018**, 1 (2018).
99. S.-K. Jeong, H.-Y. Song, S. I. Kim, T. Abe, W. S. Jeon, R.-Z. Yin, and Y. S. Kim, *Electrochem. Commun.*, **31**, 24 (2013).
100. E. Peled, D. Golodnitsky, C. Menachem, and D. Bar-Tow, *J. Electrochem. Soc.*, **145**, 3482 (1998).
101. P. M. Attia, *First Cycle SEI on Carbon Black* (2021).